

University of Nebraska - Lincoln

DigitalCommons@University of Nebraska - Lincoln

Student Research Projects, Dissertations, and
Theses - Chemistry Department

Chemistry, Department of

Fall 12-13-2019

C(sp²)-C(sp³) Cross-Coupling of Aryl Halides and Active C(sp³)-H Bonds via Dual Catalysis: Organic Photocatalysis/Nickel Redox Catalysis

Nicholas Armada

University of Nebraska - Lincoln, nicarmada@gmail.com

Follow this and additional works at: <https://digitalcommons.unl.edu/chemistrydiss>

 Part of the [Organic Chemistry Commons](#)

Armada, Nicholas, "C(sp²)-C(sp³) Cross-Coupling of Aryl Halides and Active C(sp³)-H Bonds via Dual Catalysis: Organic Photocatalysis/Nickel Redox Catalysis" (2019). *Student Research Projects, Dissertations, and Theses - Chemistry Department*. 100.
<https://digitalcommons.unl.edu/chemistrydiss/100>

This Article is brought to you for free and open access by the Chemistry, Department of at DigitalCommons@University of Nebraska - Lincoln. It has been accepted for inclusion in Student Research Projects, Dissertations, and Theses - Chemistry Department by an authorized administrator of DigitalCommons@University of Nebraska - Lincoln.

C(sp²)–C(sp³) CROSS-COUPPLING OF ARYL HALIDES AND ACTIVE C(sp³)–H
BONDS VIA DUAL CATALYSIS: ORGANIC PHOTOCATALYSIS/NICKEL
REDOX CATALYSIS

by

Nicholas Armada

A THESIS

Presented to the Faculty of
The Graduate College at the University of Nebraska
in Partial Fulfillment of the Requirements
For the Degree of Master of Science

Major: Chemistry

Under the Supervision of Professor Jian Zhang

Lincoln, Nebraska

December, 2019

C(sp²)-C(sp³) CROSS-COUPLING OF ARYL HALIDES AND ACTIVE C(sp³)-H
BONDS VIA DUAL CATALYSIS: ORGANIC PHOTOCATALYSIS/NICKEL
REDOX CATALYSIS

Nicholas Armada, M.S.

University of Nebraska, 2019

Advisor: Jian Zhang

Convenient catalytic methodologies that can facilitate the formation of C-C bonds are undoubtedly of great interest in synthetic organic chemistry. Recent reports in literature have showcased hybrid catalytic methods that couple Ni-redox catalysis and photocatalysis to enable C-H activation of tetrahydrofuran (THF) and subsequent cross-coupling with aryl halides in appreciable yields and under relatively mild reaction conditions.¹⁻² However, these studies used expensive, heavy metal-containing photocatalysts and both report difficulty obtaining low-specificity across their scopes of aryl-halides. The following report will shed light on a class of photo-excitable small organic molecules that – in conjunction with a catalytic Ni-redox cycle – can be used to catalyze C-C cross-coupling reactions between THF and aryl chlorides, bromides, and iodides with yields comparable to the aforementioned reports. After screening several organic molecules with suspected photoactivity and optimization of the reaction conditions, several benzophenone derivatives were found to catalyze the cross-coupling reaction in yields up to 97%. Mechanistic investigations suggest that this reaction proceeds through a tandem catalytic pathway that involves a photocatalyzed hydrogen atom transfer/proton-coupled electron transfer (HAT/PCET) process and a Ni-mediated oxidative addition/reductive elimination cross-coupling process.

Table of Contents

| | |
|--|----|
| Chapter 1 Introduction | 5 |
| 1.1 Cross-Coupling and Recent Photocatalytic Strategies | 5 |
| 1.2 Organic Dyes in Photocatalysis | 10 |
| 1.3 Goal of Current Study and Preliminary Design Plan | 10 |
| Chapter 2 Reaction Design, Proposed Mechanism, Reaction Optimization, and Substrate Scope of C(sp ²)-C(sp ³) Cross-Coupling | 13 |
| 2.1 Initial Investigation and Proposed Mechanism | 13 |
| 2.2 Results and Discussion | 16 |
| 2.2.1 Control Experiments | 16 |
| 2.2.2 Optimization of Nickel Catalyst | 17 |
| 2.2.3 Light Source Screening | 22 |
| 2.2.4 Optimization of Base | 23 |
| 2.2.5 Optimization of Photocatalyst | 26 |
| 2.2.6 Nickel Ligand Screening | 28 |
| 2.2.7 Scope of Aryl Halides | 29 |
| 2.2.8 Reaction Kinetics and Mechanistic Insights | 37 |
| 2.3 Experimental | 39 |
| 2.3.1 General reagents, instrumentation, and experimental procedures | 39 |
| 2.3.2 Synthesis of Photocatalysts | 40 |
| 2.2.3 Synthesis of Ni(NO ₃) ₂ dtbbpy | 41 |
| 2.4 Conclusions and Future Direction | 42 |
| Appendix A | 44 |

Chapter 1 Introduction

1.1 Cross-Coupling and Recent Photocatalytic Strategies

Given the vast applications of synthesized organic molecules, C-C bond forming methodologies are continually being discovered and refined. C-C cross-coupling reactions mediated by transition metal redox catalysis have become convention in organic synthesis. A few famous examples include the palladium catalyzed Suzuki-Miyaura, Heck, and Sonogashira reactions. These reactions exploit the oxidative nature of aryl halide and aryl boronic acid bonds, and active C-H bonds like those found in alkenes and terminal alkynes to create a variety C-C bonded products.

However, the C-H bonds used as coupling targets in the Heck and Sonogashira reactions are sp^2 and sp hybridized, respectively. For cost mitigation and convenience, C-H activation methodologies that can utilize more stable $C(sp^3)$ -H bonds as coupling targets have been a recent area of development in organic synthesis. These approaches involve specific reaction conditions that weaken a stable C-H bond in an inexpensive chemical feedstock so that it may subsequently be used in C-C bond formation.

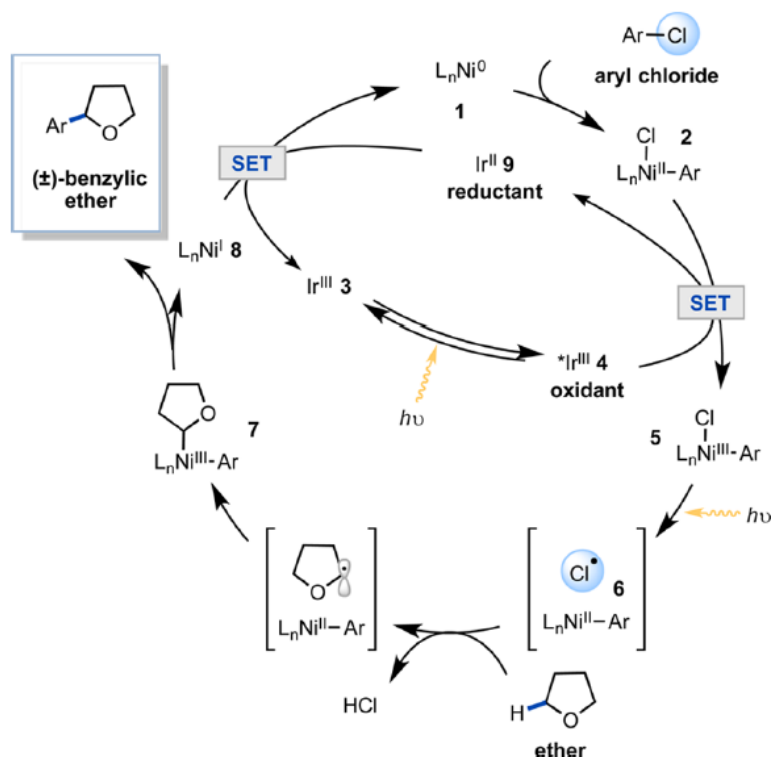
Many of these methodologies typically use heavy metals such as ruthenium³⁻⁴, rhodium⁵⁻⁶, and palladium⁷⁻⁸ to initiate bond activation. For a synthesis-heavy industry such as pharmaceutical manufacture, this drives up operating costs and often results in contamination of medicinal products.⁹⁻¹⁰ Palladium contamination of pharmaceuticals is especially common.¹¹ This is concerning because even trace amounts of heavy metals present a toxicity risk. While there are similar methodologies that use lighter metals like cobalt, nickel, and copper, they typically involve the use of stoichiometric oxidants to help push the reaction forward, which presents environmental and safety concerns.

Numerous photocatalytic methods have been shown to enable several C-C¹²⁻¹³, C-O¹⁴, and C-N¹⁵ forming reactions through C-H activation under relatively mild reaction conditions.¹⁶ Several examples in literature have also shown reaction methodologies that merge photocatalysis with transition-metal catalysis using redox cycles of palladium¹⁷⁻¹⁹, nickel²⁰⁻²¹, copper²²⁻²⁵, gold²⁶⁻²⁷, and cobalt²⁸. By utilizing photo-induced electronic excited states in a catalytic fashion, access to unique reactive intermediates can often be obtained in the absence of harsh reaction conditions such as high temperatures or stoichiometric equivalents of strong oxidants or reductants. Merging photocatalysis with traditional transition-metal catalysis makes available a variety of different possibilities for light-powered synthetic approaches.

Recent efforts by the Molander and Doyle groups have showcased photocatalytic methodologies coupled with nickel-redox catalysis that can efficiently catalyze cross-coupling between substrates with C(sp³)-H bonds such as those contained within ethers, amides, and derivatives of toluene with aryl halides using iridium-centered photocatalysts Ir[dF(CF₃)ppy]₂bpy]PF₆ and Ir[dF(CF₃)ppy]₂dtbbpy]PF₆.¹⁻² Interestingly, both groups report very different mechanisms despite their iridium catalysts having seemingly similar photophysical properties. The Doyle group proposes a mechanistic pathway that involves photoredox (Scheme 2), and the Molander group proposes a mechanistic pathway that involves only photocatalytic energy transfer (EnT) (Scheme 3).

The mechanism proposed by the Doyle group starts with a Ni(0) source, which undergoes oxidative addition by an aryl chloride to form a Ni(II) complex that can be oxidized by the excited state Ir(III) complex to form a Ni(III) complex and an Ir(II) complex. The Ni(III) complex is purported to undergo homolytic Ni-Cl bond cleavage

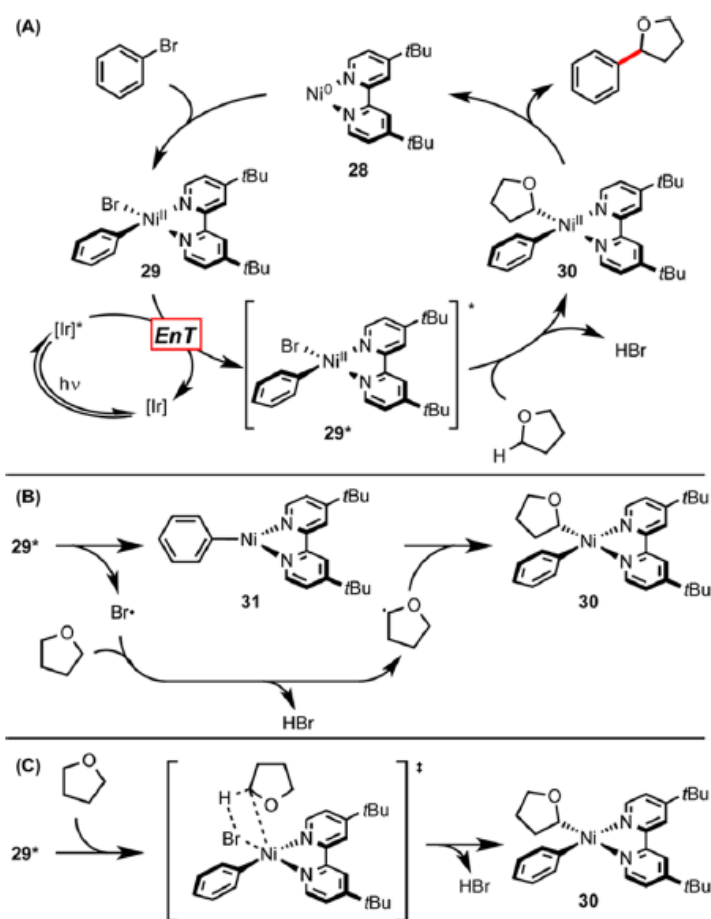
upon absorption of light, forming a Ni(II) complex as well as a chlorine radical that activates the C-H bond of THF by abstracting a hydrogen atom and subsequently forming H-Cl as a byproduct. The THF radical can add to the Ni(II) complex to form a Ni(III) complex with the aryl group that can subsequently undergo reductive elimination to form the cross-coupled product as well as a Ni(I) complex. To complete both the photocatalytic and Ni redox cycles, the Ir(II) complex reduces the remaining Ni(I) complex back to the original Ni(0) complex.



Scheme 1. Mechanistic pathway for photocatalytic C(sp²)-C(sp³) cross-coupling proposed by the Doyle group.² (Reprinted (adapted) with permission from (*J Am Chem Soc* **2016**, 138 (39), 12719-12722). Copyright (2016) American Chemical Society).

Conversely, the Molander group starts with a Ni(II) source, which presumably undergoes a series of reductions by the photocatalyst until it reaches Ni(0) so that the aryl

bromide can oxidatively add to the complex to form a Ni(II) complex. The oxidative addition complex is purported to undergo triplet-triplet energy transfer (EnT) by the excited state photocatalyst. They propose that this excited state oxidative addition complex proceeds to create and coordinate to the THF radical by two potential possibilities: 1) by subsequent homolytic Ni-Br bond cleavage that forms a bromine radical that activates the C-H bond of THF by abstracting a hydrogen atom and subsequently forming H-Br as a byproduct (part B of Scheme 3), or 2) by concerted addition of THF to the complex and formation of H-Br as a byproduct (part C of Scheme 3). Either pathway leads to a Ni(II) complex that can undergo reductive elimination to form the cross-coupled product and complete the Ni redox cycle by regenerating Ni(0).



Scheme 2. Mechanistic pathway for photocatalytic C(sp²)-C(sp³) cross-coupling proposed by the Molander group.¹ (*J Am Chem Soc* **2016**, 138 (39), 12715-12718). Copyright (2016) American Chemical Society).

These methods are noteworthy because they use cheap and abundant nickel to mediate cross-coupling. However, one important and practical limitation of these methodologies is that they use photocatalysts that contain iridium at their centers. While these catalysts provide easy access to useful excited states, they – as well as their synthetic precursors – carry a hefty price tag since metals like iridium exist in low natural abundances and often require extensive mining processes to obtain.

1.2 Organic Dyes in Photocatalysis

A number of published studies have demonstrated the viability of small organic molecules that contain chromophores capable of producing similarly useful excited states at a fraction of the cost of heavy metal-centered photocatalysts. One specific class of organic compounds that have found promising value in photoredox applications are those with donor-acceptor (D-A) properties. In their excited states, these organic molecules mimic the type of charge transfer process that occurs in the excited state of metal complexes like $\text{Ru}(\text{bpy})_3^{2+}$, which is often touted as the prototypical photoredox catalyst for organic synthesis. One popular example is $\text{Acr}^+\text{-Mes}$, which has an excited state oxidation potential of +1.88 V that is surprisingly high enough to oxidize water.²⁹ Our group has recently published an account showcasing a variety of carbazole-substituted dicyanobenzenes that possess varying photoredox properties in their excited states.³⁰ Another class of organic molecules with interesting photochemical properties are diaryl ketones such as benzophenone, which has been long known to be able to provoke hydrogen atom transfer processes photochemically.³¹ The success of this photoinduced bond homolysis by diaryl ketones is due to the (n,π^*) electronic transition that occurs during photoexcitation. The triplet (n,π^*) excited state opens many avenues for photocatalytic processes such as proton-coupled electron transfer (PCET), hydrogen atom transfer (HAT), and single-electron transfer (SET).³²⁻³³

1.3 Goal of Current Study and Preliminary Design Plan

The current study aims to develop a similar $\text{C}(\text{sp}^2)\text{-C}(\text{sp}^3)$ cross-coupling methodology to those reported by Doyle and Molander that can utilize a small organic

molecule in place of an iridium-centered complex as the photocatalyst. This would be an attempt to reduce the overall cost of this transformation by adapting the properties of an inexpensive organic photocatalyst to the method. In choosing a suitable molecule to function as the photocatalyst in this type of system, there are two main mechanistic barriers to overcome: 1) creation of a THF radical, and 2) propagation of a catalytic redox cycle of nickel.

One point of initial interest was the organic co-catalyst, bis-4-methoxybenzophenone (b4MeOBP), that was used in the Molander group's study. The benzophenone-derived co-catalyst was thought to aid in the reaction by creating carbon-centered THF radicals through HAT. We also looked to a recent study in our group that found a group of substituted benzophenones that were successful in generating phthalimide-N-oxyl (PINO) radicals from N-hydroxyphthalimide (NHPI) through proton-coupled electron transfer in the presence of visible light.³² The bond dissociation energy (BDE) of the O–H bond in NHPI is 88 kcal/mol and the BDE of the C–H bond in THF is 92 kcal/mol. With this in mind, we thought that this class of catalysts may be able to directly abstract a hydrogen atom from THF to form the THF radical that could be used in a nickel-mediated cross-coupling with an aryl halide. After HAT, the photocatalyst would exist as a carbon-centered alpha-hydroxy radical. Electrochemical measurements of $E_{1/2}(M/M^{\cdot-})$ for b4CzBP (-1.68 V vs SCE), b4DPABP (-1.77 V vs SCE), and 4DMABP (-2.16 V vs SCE) – which correspond to the reduction potentials of their associated ketyl radical anions – indicate that subsequent deprotonation of the alpha-hydroxy radical formed from these substituted-benzophenones could produce a photocatalyst species

reductive enough to reduce Ni(II) to Ni(I), and Ni(I) to Ni(0) via a series of single electron transfer processes.³²

Chapter 2 Reaction Design, Proposed Mechanism, Reaction Optimization, and Substrate Scope of C(sp²)-C(sp³) Cross-Coupling

2.1 Initial Investigation and Proposed Mechanism

We began our investigation by first screening a variety of photoactive organic donor-acceptor fluorophores (Figure 1) against Ir[dF(CF₃)ppy]₂dtbbpy]PF₆ as a control. The reaction conditions published by the Molander group were used, as they used a bench-stable nickel (ii) source, Ni(NO₃)₂·6H₂O.

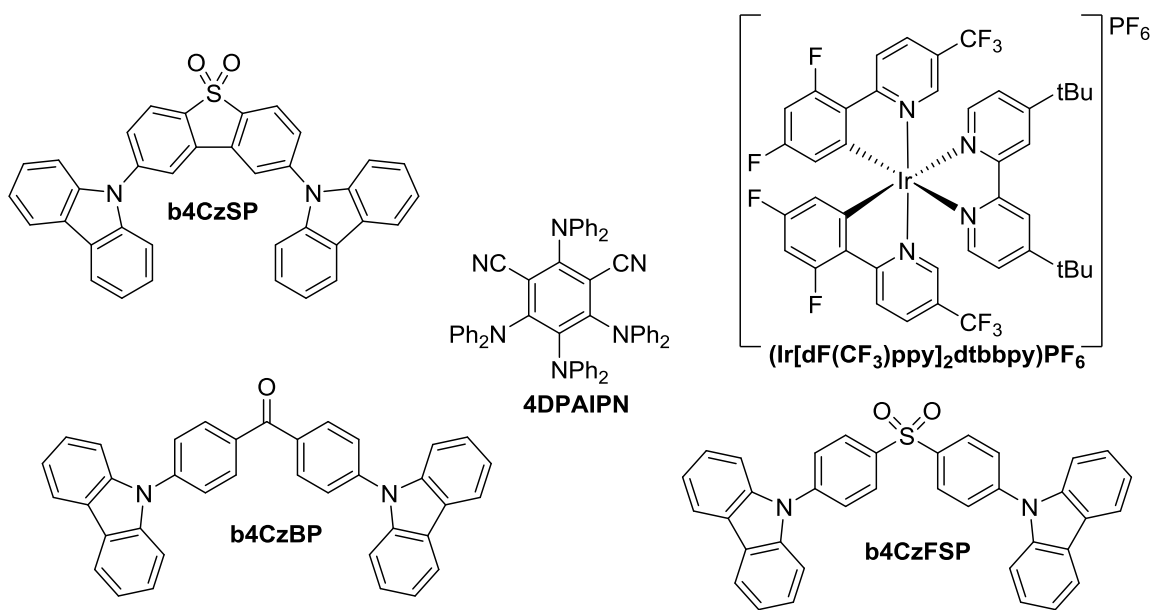
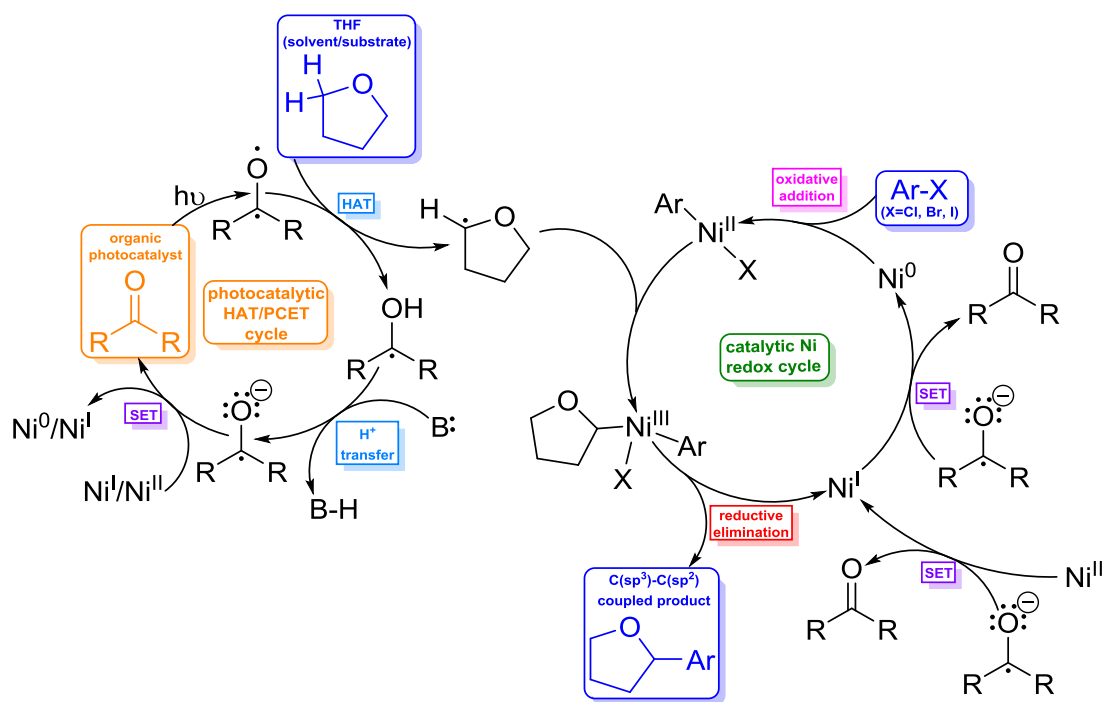


Figure 1. Structures of preliminary photocatalyst screening.

Out of the organic photocatalyst candidates initially screened, only b4CzBP and Ir[dF(CF₃)ppy]₂dtbbpy]PF₆ produced products. The appearance of a new spot with the same R_f value upon thin-layer chromatography analysis of both crude reaction mixtures indicated that 4-bis-carbazolebenzophenone (b4CzBP) could be a viable alternative to

Ir[dF(CF₃)ppy]₂dtbbpy]PF₆ as a photocatalyst. Formation of the desired product for both reactions was verified via ¹H NMR (Figures X and X). Yields of 57% and 64% for the reactions with b4CzBP and Ir[dF(CF₃)ppy]₂dtbbpy]PF₆, respectively, were determined using ¹H NMR and 2,4,6-trimethoxybenzonitrile as an internal standard. Isolated yields of 50% and 67% were obtained for the reactions with b4CzBP and Ir[dF(CF₃)ppy]₂dtbbpy]PF₆, respectively, via column chromatography (Figures X and X).

A plausible mechanism for the success of b4CzBP in this reaction has been proposed in Scheme 2. The photocatalytic cycle begins with the photocatalyst absorbing a photon and accessing a triplet excited state through intersystem crossing (ISC), where it can abstract a hydrogen atom from THF, forming a THF radical and an alpha-hydroxy radical. In the presence of base, the alpha-hydroxy radical can be deprotonated to form a ketyl radical anion, which can be subsequently oxidized by Ni(II) or Ni(I) to regenerate the ground state photocatalyst and complete the photocatalytic cycle. At the beginning of the nickel redox cycle, Ni(II) can be reduced to Ni(I), and subsequently to Ni(0) ($E_{1/2}(\text{Ni}^{\text{I}}/\text{Ni}^0) = -1.17 \text{ V vs SCE}$)² via single electron reduction by the ketyl radical anion ($E_{1/2}(\text{M}/\text{M}^-) = -1.69 \text{ V vs SCE}$).³² Once Ni(0) is present, the aryl halide can oxidatively add to it, forming a Ni(II) complex to which the THF radical formed in the photocatalytic cycle can add, forming a Ni(III) complex. Finally, this Ni(III) complex can undergo reductive elimination to form the desired C(sp³)-C(sp²) coupled product and Ni(I), which can be reduced by the ketyl radical anion to form Ni(0) to complete the Ni-redox cycle.



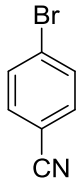
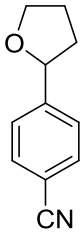
Scheme 2. Proposed reaction mechanism for the dual-catalytic cross-coupling reaction.

2.2 Results and Discussion

2.2.1 Control Experiments

A set of control reactions indicated that b4CzBP, light, base, and nickel are all necessary requirements for the reaction to proceed efficiently (Table 1).

Table 1. Control reactions showcasing necessary reaction components^[a]

| <div style="display: flex; align-items: center; justify-content: center;"> <div style="text-align: center; margin-right: 20px;">  </div> <div style="text-align: center; margin-right: 20px;"> $\xrightarrow[\text{K}_2\text{HPO}_4 \text{ (2 eq)}]{\text{b4CzBP (4.8 mol\%)}, \text{Ni(NO}_3)_2 \cdot 6\text{H}_2\text{O (4.8 mol\%)}, \text{dtbbpy (4.8 mol\%)}}$ THF $h\nu = \text{CFL}, t = 72 \text{ hrs}, T = \text{rt}$ </div> <div style="text-align: center; margin-left: 20px;">  </div> </div> | | |
|---|---------------------|------------------------|
| Entry | Control | % Yield ^[b] |
| 1 | none | 57% |
| 2 | No photocatalyst | 0% |
| 3 | No light | 0% |
| 4 | No Nickel or Ligand | 0% |
| 5 | No Ligand | Trace |
| 6 | No Base | 13% |

[a] Reaction scale: 4-bromobenzonitrile (0.12 mmol).

[b] Determined by ¹H NMR with 2,4,6-trimethoxybenzonitrile as the internal standard.

2.2.2 Optimization of Nickel Catalyst

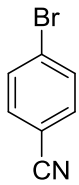
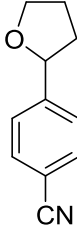
Upon setting up a batch of parallel reactions to test repeatability, a wide variability in yields that correlated with the reaction solution color was observed (Table 2). This large deviance was confirmed to be a result of the formation of the bis-ligated nickel complex, which is detrimental to the cross-coupling reaction for two reasons. First, it should be noted that the mono-ligated complex would provide the most conducive conditions for catalysis to occur since multiple ligand exchanges are expected to take place during the oxidative addition/reductive elimination steps of the catalytic nickel redox cycle. The bis-ligated complex would be expected to hinder nickel's ability to partake in catalysis due to its increased stability and steric bulk. Second, since the bis-ligated complex is less soluble in THF, its precipitation from the reaction mixture decreases the amount of nickel available for catalysis.

At first, the plan was to prepare the mono-ligated nickel complex by heating a 1:1 ratio solution of $\text{Ni}(\text{NO}_3)_2 \cdot 6\text{H}_2\text{O}$ and dtbbpy in THF, as the Molander group did in their study.¹ The resulting solution is blue in color (Figure 2). However, as this solution cools to room temperature and sits undisturbed for an additional 30 minutes, purple crystals begin to precipitate (Figure 2b). Single-crystal X-ray diffraction experiments (Figure X) confirmed that these purple crystals were indeed the bis-ligated nickel complex.

It was found that the preparation of the nickel complex *in situ* with a 2:3 molar ratio of [dtbbpy]: $[\text{Ni}(\text{NO}_3)_2 \cdot 6\text{H}_2\text{O}]$ produced the best cross-coupling yields (Table 3). Additionally, the mono-ligated complex was successfully isolated from a nickel/ligand solution containing 1.5 eq $\text{Ni}(\text{NO}_3)_2 \cdot 6\text{H}_2\text{O}$ (Figure 2a) and subsequently characterized via single-crystal x-ray diffraction (Figure X). Adding this purified complex to the reaction

vessel as a solid in an equimolar concentration to the photocatalyst ensured cross-coupling yield consistency (Table 4).

Table 2. Yield variations dependent on reaction solution color^[a]

| <div style="display: flex; align-items: center; justify-content: center;"> <div style="text-align: center; margin-right: 20px;">  </div> <div style="text-align: center; margin-right: 20px;"> $\xrightarrow[\text{K}_2\text{HPO}_4 \text{ (2 eq)}]{\text{b4CzBP (4.8 mol\%)}, \text{Ni(NO}_3)_2 \cdot 6\text{H}_2\text{O (4.8 mol\%)}, \text{dtbbpy (4.8 mol\%)}}$ THF $h\nu = \text{CFL}, t = 72 \text{ hrs}, T = \text{rt}$ </div> <div style="text-align: center; margin-left: 20px;">  </div> </div> | | |
|---|----------------|------------------------|
| Entry | Solution Color | % Yield ^[b] |
| 1 | Cloudy white | 20% |
| 2 | Cloudy green | 38% |
| 3 | Cloudy blue | 41% |
| 4 | Clear blue | 57% |
| 5 | Clear blue | 62% |
| 6 | Cloudy pink | 18% |
| 7 | Cloudy pink | 14% |
| 8 | Cloudy pink | 19% |

[a] Reaction scale: 4-bromobenzonitrile (0.12 mmol).
[b] Determined by ¹H NMR with 2,4,6-trimethoxybenzonitrile as the internal standard.

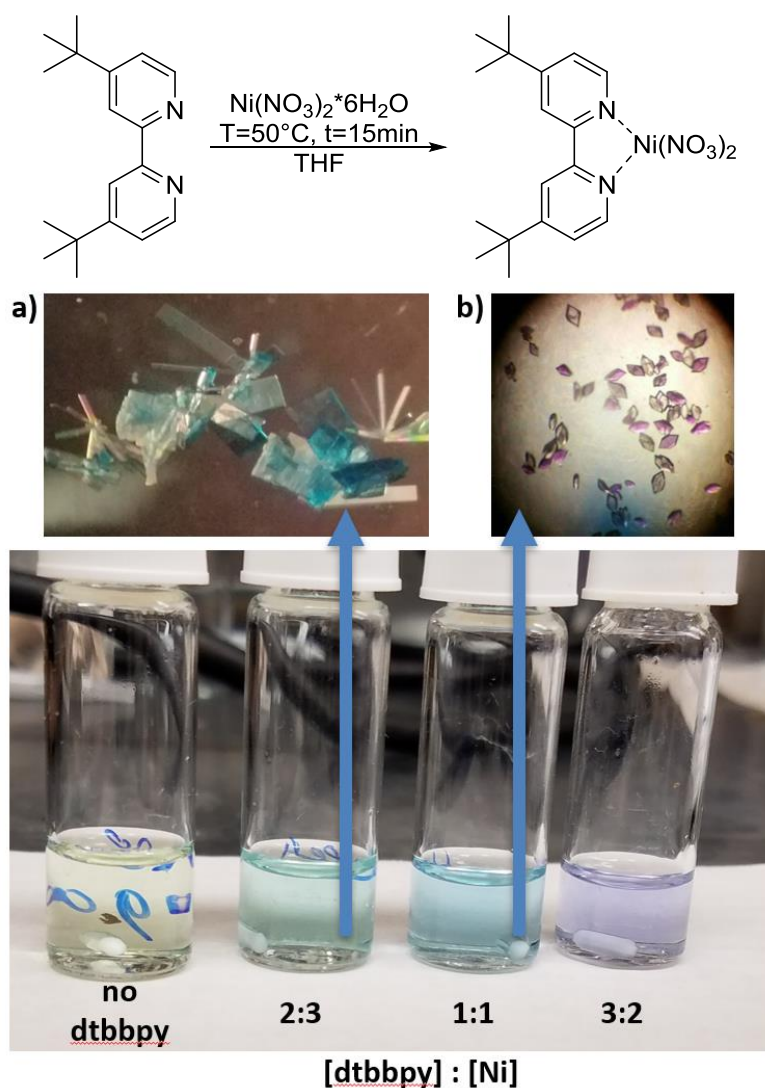
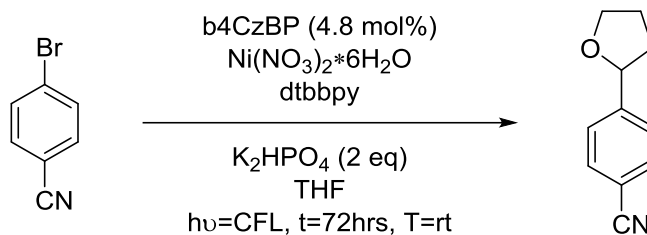


Figure 2. Solution color dependence on molar ratio of [dtbbpy]:[Ni(NO₃)₂·6H₂O].

a) Crystal photos of the mono-ligated complex prepared from the 2:3 solution.

b) Crystal photos of the bis-ligated complex that precipitated from the 1:1 solution.

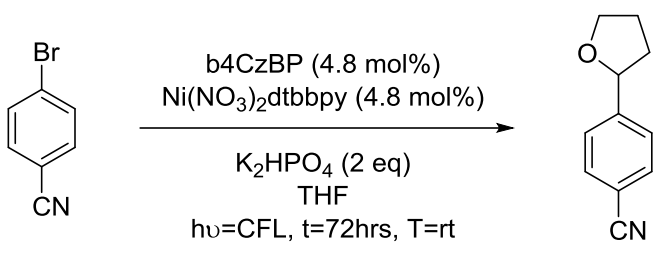
Table 3. Reaction yield dependence on molar ratio of [dtbbpy]:[Ni(NO₃)₂·6H₂O]^[a]

| Entry | dtbbpy | Ni(NO ₃) ₂ ·6H ₂ O | %Yield ^[b] |
|-------|----------|--|-----------------------|
| 1 | 0 mol% | 4.8 mol% | Trace |
| 2 | 4.8 mol% | 7.2 mol% | 61% |
| 3 | 4.8 mol% | 4.8 mol% | 31% |
| 4 | 7.2 mol% | 4.8 mol% | 33% |

[a] Reaction scale: 4-bromobenzonitrile (0.12 mmol).

[b] Determined by ¹H NMR with 2,4,6-trimethoxybenzonitrile as the internal standard. Yields shown are averages of two trials per entry.

Table 4. Improvement in reaction yield consistency using synthesized nickel complex

|  | |
|--|--------------------------|
| Entry | % Yield ^[b] |
| 1 | 45% |
| 2 | 55% |
| 3 | 57% |
| 4 | 40% |
| 5 | 43% |
| 6 | 49% |
| 7 | 51% |
| Average | 49%^[c] |
| <p>[a] Reaction scale: 4-bromobenzonitrile (0.12 mmol). [b] Determined by ¹H NMR with 2,4,6-trimethoxybenzonitrile as the internal standard.</p> <p>[c] Standard deviation = ±6%</p> | |

To further optimize the reaction yields, a variety of light sources were screened (Table 5): purple LED strips, blue LED strips, a non-UV white LED bulb, and a compact fluorescent lamp (CFL) bulb. The white CFL bulb, purple LEDs, blue LEDs, and non-UV white LED bulb were found to produce yields of 46% ±6%, 78% ±10%, 0%, and 0%, respectively. The emission spectra of the light sources used and the UV-Vis absorption spectra for b4CzBP and dibenzosuberone (DBS) are shown in Figure 3.

2.2.3 Light Source Screening

Table 5. Reaction yield improvement with higher energy photons.

| <chem>N#Cc1ccc(Br)cc1</chem> $\xrightarrow[\text{K}_2\text{HPO}_4 \text{ (2 eq), THF, } h\nu = \text{light source, } t = 72 \text{ hrs, } T = \text{rt}}]{\text{b4CzBP (4.8 mol\%), Ni(NO}_3)_2\text{dtbbpy (4.8 mol\%)}}$ <chem>N#Cc1ccc(C2OCC2)cc1</chem> | |
|---|------------------------------|
| Light Source | % Yield ^[b] (n=3) |
| CFL | 46% \pm 6% |
| Purple LEDs | 78% \pm 10% |
| Blue LEDs | 0% |
| UV-free LED bulb | 0% |

[a] Reaction scale: 4-bromobenzonitrile (0.12 mmol).

[b] Determined by ¹H NMR with 2,4,6-trimethoxybenzonitrile as the internal standard.

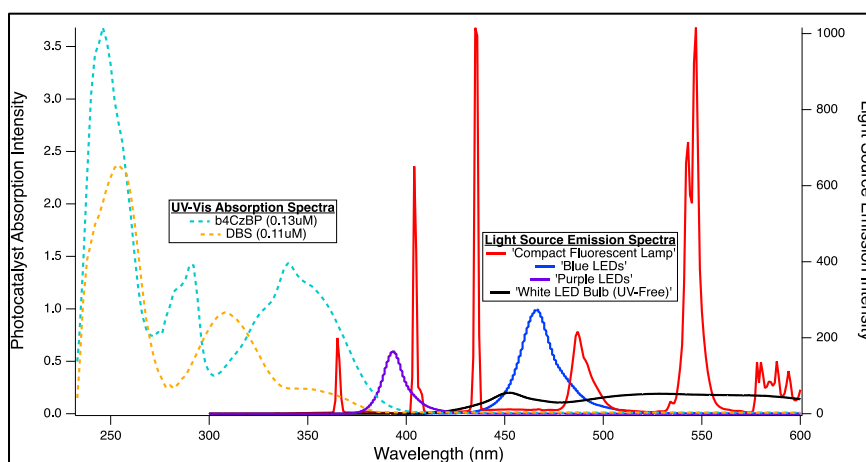


Figure 3. Emission spectra for blue LEDs, purple LEDs, and white CFL bulb

2.2.4 Optimization of Base

We were pleased to observe a massive increase in reaction yield when increasing the strength of the base (Table 6). This stark difference in reaction yield makes sense, since we propose that the base is directly involved in the catalytic cycle rather than simply serving to neutralize the resulting H-X. Considering the reversibility of the proton transfer step, too weak of a base could certainly hinder the success of the reaction (Scheme 3).

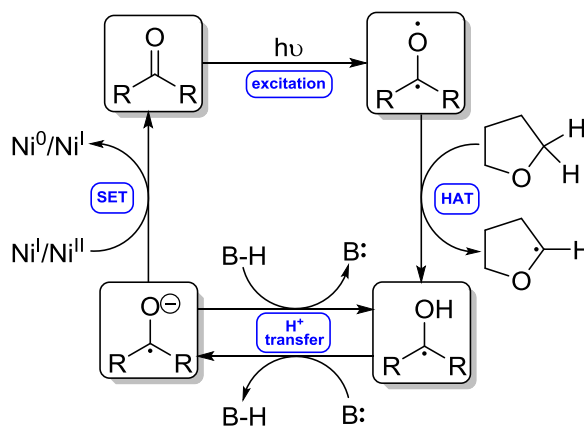
Considering the results of the light source screening, the base optimization experiments were run with purple LEDs and with a CFL. Interestingly, the yields after optimizing the base choice were observed to be slightly higher with a CFL light source as opposed to the purple LEDs.

Table 6. Strong dependence of reaction yield on base choice^[a]

| Base | %Yield (CFL) ^[b] | %Yield (purple LEDs) ^[b] |
|---------------------------------|-----------------------------|-------------------------------------|
| Na ₂ CO ₃ | 94% | 92% |
| K ₂ CO ₃ | 90% | 87% |
| K ₂ HPO ₄ | 35% | 33% |
| K ₃ PO ₄ | 91% | 88% |

[a] Reaction scale: 4-bromobenzonitrile (0.12 mmol).

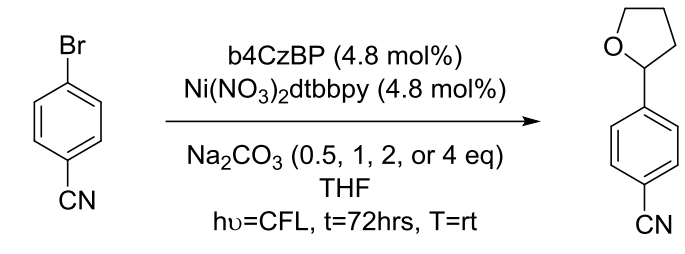
[b] Determined by ¹H NMR with 2,4,6-trimethoxybenzonitrile as the internal standard.

**Scheme 3.** Proposed HAT/PCET photocatalytic pathway with direct base involvement.

After selecting Na₂CO₃ as the optimum base, a set of reactions were run to screen the effect of base loading on the reaction (Table 7). Base loadings below 2 eq were found

to hinder reaction yields, and base loadings above 2 eq were found to not have any significant effect on yield.

Table 7. Screening of base loading^[a]

|  | |
|--|-----------------------------|
| Na₂CO₃ Loading | %Yield^[b] |
| 0.5 eq | 23% |
| 1 eq | 39% |
| 2 eq | 94% |
| 4 eq | 93% |

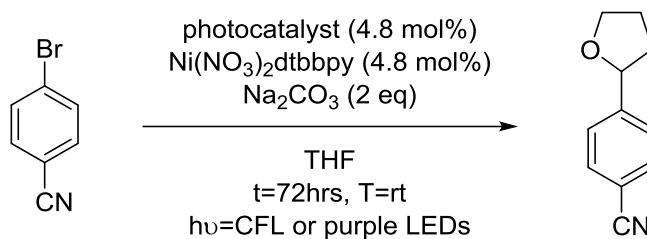
[a] Reaction scale: 4-bromobenzonitrile (0.12 mmol).

[b] Determined by ¹H NMR with 2,4,6-trimethoxybenzonitrile as the internal standard.

2.2.5 Optimization of Photocatalyst

In an effort to uncover any other types of organic ketones might find success in our optimized system, a second photocatalyst screening was run to evaluate other types of benzophenone derivatives (Table 7). During the course of our investigation, reports were published of 4-MeO-4'-CF₃ BP and b4ClBP performing a very similar reaction to the one presented in this study.³⁴⁻³⁵ As such, they were also included in this screening study for comparative analysis. Yields upward of 90% were observed for DBS and b4CzBP and yields upward of 70% were observed for 4-MeO-4-CF₃ BP and b4ClBP. An appreciable yield of 62% was observed for 4-benzoylpyridine, and a yield of 35% was observed for b4MeOBP – the ketone used as a co-catalyst to Ir[dF(CF₃)ppy]₂bpy]PF₆ in the study done by the Molander group.¹

Table 7. Screening of benzophenone-derived photocatalysts with CFL or purple LEDs as light sources^[a]



| Photocatalyst | %Yield ^[b] (CFL) | %Yield ^[b] (purple LEDs) |
|----------------------------|-----------------------------|-------------------------------------|
| b4CzBP | 97% | 95% |
| DBS | 94% | 91% |
| 4-MeO-4-CF ₃ BP | 71% | n/a |
| b4ClBP | 70% | n/a |
| 4-benzoylpyridine | 62% | 59% |
| b4MeOBP | 35% | 33% |
| Benzophenone | 12% | 9% |
| Acridone | 0% | 0% |
| Xanthone | 0% | 0% |
| 9-fluorenone | 0% | 0% |

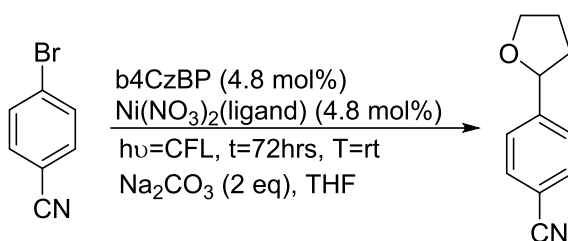
[a] Reaction scale: 4-bromobenzonitrile (0.12 mmol).

[b] Determined by ¹H NMR with 2,4,6-trimethoxybenzonitrile as the internal standard.

2.2.6 Nickel Ligand Screening

The study by Shen et al reported to have increased success with (m-Me)bpy compared to dtbbpy as the nickel ligand.³⁴ This prompted a screening of three other variants of the bipyridine ligand (Table 8). However, dtbbpy remained the best choice to ligate nickel our reaction system.

Table 8. Screening of Nickel Ligand^[a]



| Entry | Ligand | Structure | % Yield ^[b] |
|-------|-----------|-----------|------------------------|
| 1 | dtbbpy | | 94% |
| 2 | (m-Me)bpy | | 34% |
| 3 | (o-Me)bpy | | 19% |
| 4 | bpy | | 9% |

[a] Reaction scale: 4-bromobenzonitrile (0.12 mmol).

[b] Determined by ¹H NMR with 2,4,6-trimethoxybenzonitrile as the internal standard.

2.2.7 Scope of Aryl Halides

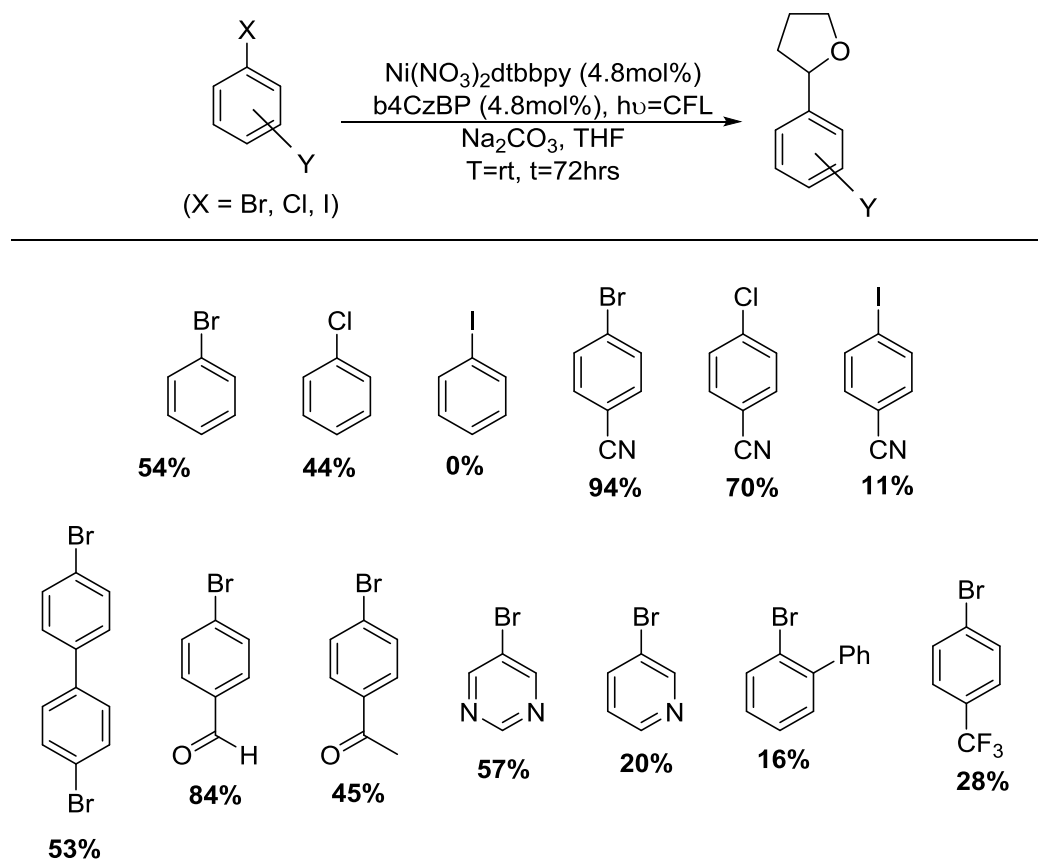
Next, we sought to test the substrate scope of aryl-halides (Table 9). In general, aryl bromides produced the best yield results, while aryl chlorides produced moderate yields. Conversely, aryl iodides produced the poorest yields. The reaction of 4-bromobenzonitrile was found to attain a yield of 94% in just 48 hours of reaction time, as well as an 84% yield in 90 hours of reaction time under an air atmosphere (Table 10).

In an attempt to raise the yields of aryl chlorides and aryl iodides, a screening of tetrabutylammonium halide (TBA-X) additives at various concentrations was conducted (Tables 11-14). Adding TBA-Br drastically improved the yield of the reaction of 4-chlorobenzonitrile and THF, but had little effect on the yield with 4-iodobenzonitrile as a substrate (Figure 4). Adding TBA-Br to the reaction with 4-bromobenzonitrile decreased the yield from 97% without the additive, to 35% with it. Also, adding TBA-I decreased the yields for all 4-halonitrile substrates (Figure 5). The optimum loading of TBA-Br to increase the yield of the reaction using 4-chlorobenzonitrile was found to be 0.5 eq, increasing the yield from 59% without TBA-Br, to 94% with the additive. A dependence on TBA-Br loading and the yield of coupled product was elucidated for 4-chlorobenzonitrile. Increasing the TBA-Br loading to past 0.5 equivalents to 1 equivalent still increased yield of coupled product to 85%, but TBA-Br was observed to be supersaturated in THF at this loading, which may be the reason why the yield is higher with a 0.5 eq loading.

In the case of aryl iodides, the reductive elimination step may be where the reaction fails. This presumption is based on the observation of the reaction color of the aryl iodide reactions changing from a clear blue to orange after about 24 hours of

exposure to the light source. This is also considering that the oxidative addition complex – which forms readily with $\text{Ni}(\text{cod})_2$ and 4-iodobenzonitrile – is orange in color. This hypothesis is further supported by the fact that the reaction solution with 4-bromobenzonitrile – which typically appears a faint yellow after 72 hours of reaction time under the standard conditions – also changes from clear blue to orange after 24 hours of exposure to the light source in the presence of the TBA-I additive (Figure 6)

Table 9. Substrate Scope of Aryl Halides^[a]



[a] Reaction scale: 4-bromobenzonitrile (0.12 mmol). Yields determined by ^1H NMR with 2,4,6-trimethoxybenzonitrile as the internal standard.

Table 10. 48 hour time point and air atmosphere reaction with 4-bromobenzonitrile^[a]

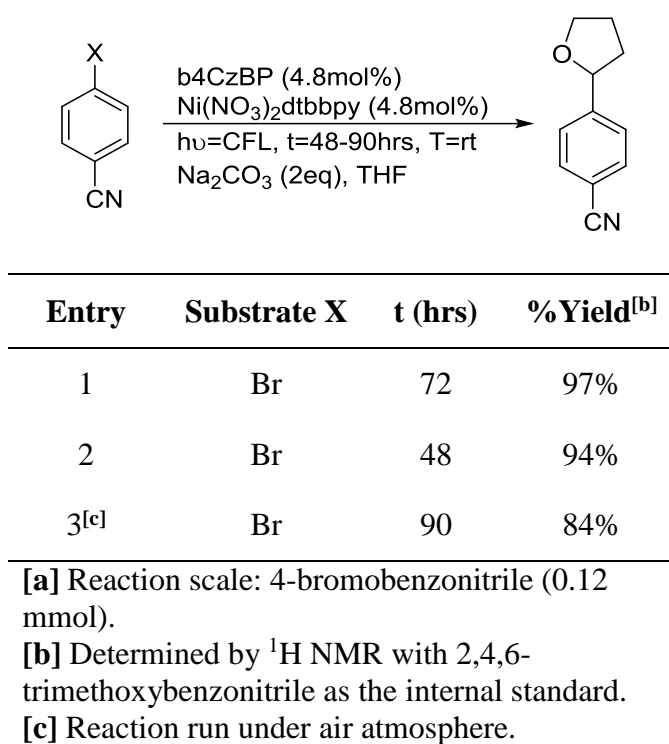
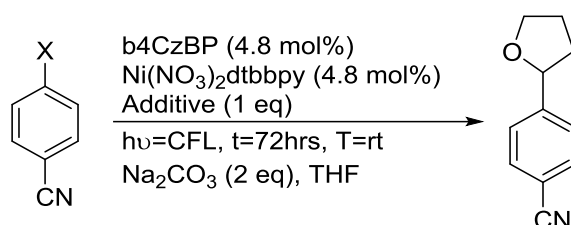


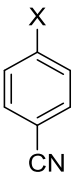
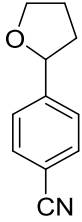
Table 11. Screening of tetrabutylammonium-halide additives (1 eq)^[a]



| Entry | Additive | Substrate X | %Yield ^[b] |
|-------|----------|-------------|-----------------------|
| 1 | TBA-Br | Br | 42% |
| 2 | TBA-Br | Cl | 85% |
| 3 | TBA-Br | I | 11% |
| 4 | TBA-I | Br | trace |
| 5 | TBA-I | Cl | trace |
| 6 | TBA-I | I | trace |

[a] Reaction scale: 4-bromobenzonitrile (0.12 mmol).
 [b] Determined by ¹H NMR with 2,4,6-trimethoxybenzonitrile as the internal standard.

Table 12. Screening of tetrabutylammonium-halide additives (0.5 eq)^[a]

| <div style="display: flex; align-items: center; justify-content: space-around;"> <div style="text-align: center;">  </div> <div style="text-align: center;"> <p>b4CzBP (4.8 mol%) Ni(NO₃)₂dtbbpy (4.8 mol%) Additive (0.5 eq)</p> <hr style="width: 100%;"/> <p>hν=CFL, t=72hrs, T=rt Na₂CO₃ (2 eq), THF</p> </div> <div style="text-align: center;">  </div> </div> | | | |
|---|----------|-------------|-----------------------|
| Entry | Additive | Substrate X | %Yield ^[b] |
| 1 | TBA-Br | Br | 35% |
| 2 | TBA-Br | Cl | 94% |
| 3 | TBA-Br | I | trace |
| 4 | TBA-I | Br | trace |
| 5 | TBA-I | Cl | trace |
| 6 | TBA-I | I | trace |

[a] Reaction scale: 4-bromobenzonitrile (0.12 mmol).

[b] Determined by ¹H NMR with 2,4,6-trimethoxybenzonitrile as the internal standard.

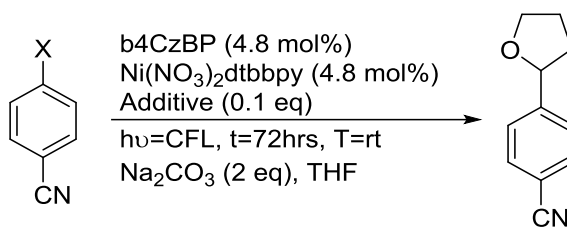
Table 13. Screening of tetrabutylammonium-halide additives (0.25 eq)^[a]

| Entry | Additive | Substrate X | %Yield ^[b] |
|-------|----------|-------------|-----------------------|
| 1 | TBA-Br | Br | 37% |
| 2 | TBA-Br | Cl | 75% |
| 3 | TBA-Br | I | trace |
| 4 | TBA-I | Br | trace |
| 5 | TBA-I | Cl | trace |
| 6 | TBA-I | I | trace |

[a] Reaction scale: 4-bromobenzonitrile (0.12 mmol).

[b] Determined by ¹H NMR with 2,4,6-trimethoxybenzonitrile as the internal standard.

Table 14. Screening of tetrabutylammonium-halide additives (0.1 eq)^[a]



| Entry | Additive | Substrate X | % Yield ^[b] |
|-------|----------|----------------|------------------------|
| 1 | TBA-Br | Br | 33% |
| 2 | TBA-Br | Cl | 50% |
| 3 | TBA-Br | I | trace |
| 4 | TBA-I | Br | trace |
| 5 | TBA-I | Cl | trace |
| 6 | TBA-I | I | trace |

[a] Reaction scale: 4-bromobenzonitrile (0.12 mmol).

[b] Determined by ¹H NMR with 2,4,6-trimethoxybenzonitrile as the internal standard.

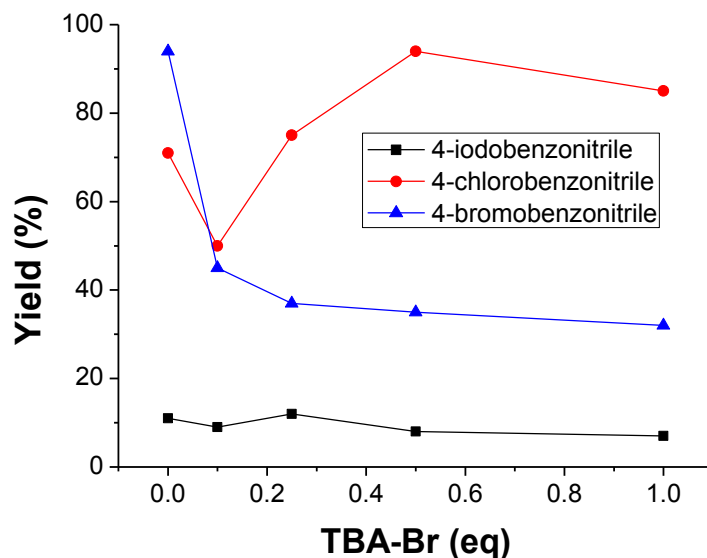


Figure 4. Effect of tetrabutylammonium-bromide loading (0.1 eq, 0.25 eq, 0.5 eq, and 1 eq) on yield with substrates 4-iodobenzonitrile, 4-chlorobenzonitrile, and 4-bromobenzonitrile (0.12 mmol scale). % Yield determined by ^1H NMR with 2,4,6-trimethoxybenzonitrile as the internal standard.

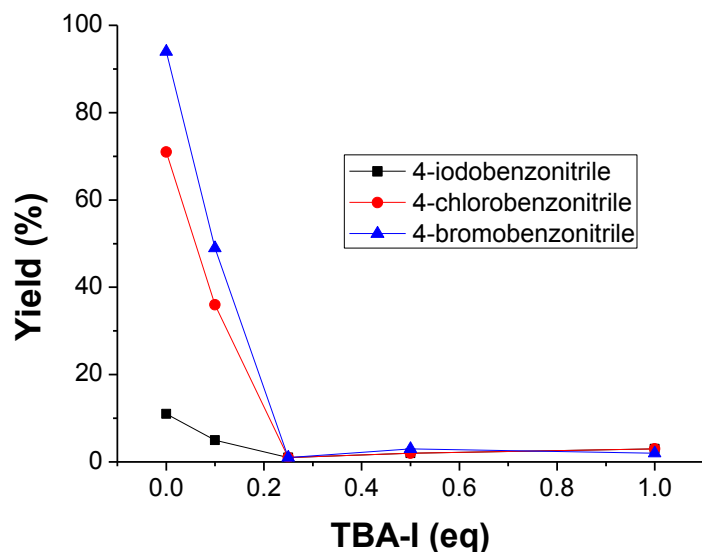


Figure 5. Effect of tetrabutylammonium-iodide loading (0.1 eq, 0.25 eq, 0.5 eq, and 1 eq) on yield with substrates 4-iodobenzonitrile, 4-chlorobenzonitrile, and 4-bromobenzonitrile (0.12 mmol scale). % Yield determined by ^1H NMR with 2,4,6-trimethoxybenzonitrile as the internal standard.

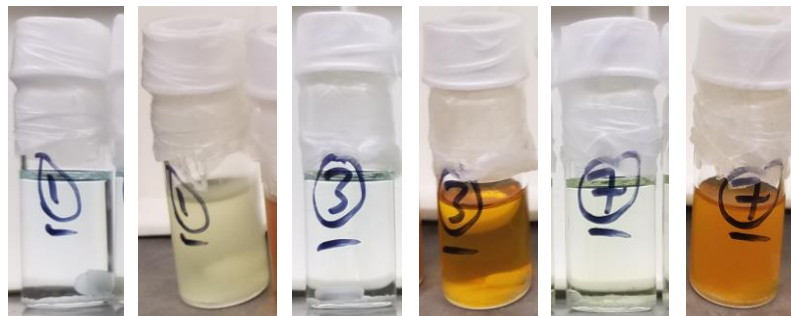


Figure 6. Reaction mixtures of 4-bromobenzonitrile (vial 1), 4-iodobenzonitrile (vial 3), and 4-bromobenzonitrile with 0.5 eq of TBA-I added (vial 7). For each pair, the left photo is at $t = 0$ hours and the right photo is at $t = 72$ hours.

2.2.8 Reaction Kinetics and Mechanistic Insights

The reaction with 4-bromobenzonitrile was run at different time points to showcase the yield progress over time with the two highest performing ketone photocatalysts in our study, b4CzBP and DBS (Figure 7). With b4CzBP, a moderate yield of 87% was observed after only 36 hours of light exposure (CFL), and nearly quantitative yields were observed after 60 hours of light exposure (CFL). With DBS, a moderate yield of 75% was observed after only 36 hours of light exposure (CFL), and a yield of 85% was observed after 60 hours of light exposure (CFL). Using purple LEDs as a light source, the yields were slightly lower for both photocatalysts.

To evaluate our hypothesis of a Ni(0) intermediate being involved in the reaction mechanism, a Ni(0) source – Ni(cod)₂ – was used in lieu of a Ni(II) source. As was observed for the Ni(II) conditions, the reaction reached near quantitative yields after 60 hours of light exposure (CFL).

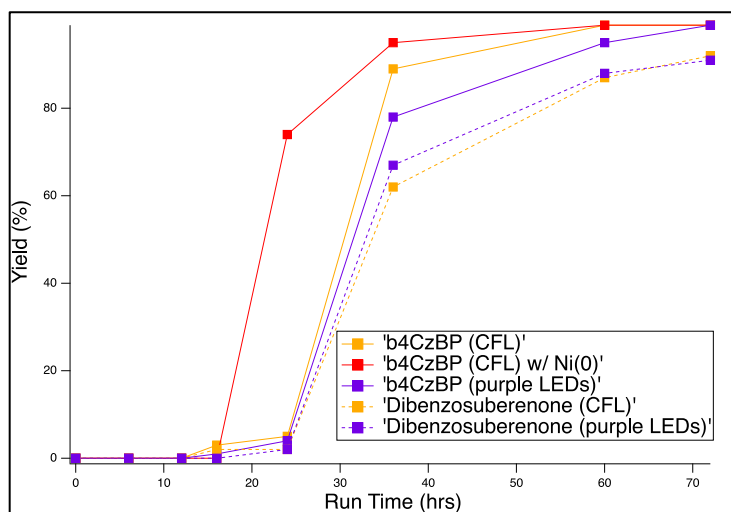


Figure 7. Kinetics data for reactions using b4CzBP or DBS as the photocatalyst, CFL or purple LEDs as the light source, and Ni(ii) or Ni(0) as the nickel source. Reaction scale: 4-bromobenzonitrile (0.12 mmol). Yields determined by ^1H NMR with 2,4,6-trimethoxybenzonitrile as the internal standard.

2.3 Experimental

2.3.1 General reagents, instrumentation, and experimental procedures

All chemical feedstocks used for catalytic reactions were purchased from commercial sources and used without further purification. ^1H NMR spectroscopy was performed on a 300 MHz or 400 MHz Bruker FT-NMR spectrometer. Fluorescence spectroscopy was performed on a Shimadzu RF-5301PC spectrofluorophotometer. UV/Vis spectroscopy was performed on a Shimadzu UV-2501PC UV-Vis recording spectrophotometer.

General procedure for photocatalytic reaction setup

A 3 mL screw-top vial was charged with a stir-bar, aryl halide (0.12 mmol, 1 eq), Na_2CO_3 (2 eq, 0.24 mmol, X mg), b4CzBP (4.8 mol%, 5.8 μmol , 1.1 mg), and $\text{Ni}(\text{NO}_3)_2\text{dtbbpy}$ (4.8 mol %, 5.8 μmol , 1.5 mg). The vial was then fitted with a septum cap and evacuated and purged with argon three times. Under an argon atmosphere, 2.3 mL of freshly distilled THF was added to the reaction vial. The reaction vial was then sonicated for 15 seconds to thoroughly dissolve the contents, and subsequently placed approximately 1 cm from a 26W CFL fixed over a magnetic stirrer. A fan was fitted above the reaction mixture to keep the temperature of the reaction at room temperature. The reaction was stirred for 36 – 72 hours. For purification of the product, THF was removed with rotary evaporation and the resulting residue dissolved in a minimal amount of DCM. One equivalent of internal standard 2,4,6-trimethoxybenzonitrile was then added to the solution and yields were determined by ^1H NMR integration of the aromatic

hydrogens on the internal standard at 6.02 ppm (s, 2H) to the benzylic proton on the associated product that appears around 4.9 ppm (t, 1H).

2.3.2 Synthesis of Photocatalysts

bis(4-carbazol-9-ylphenyl)methanone (b4CzBP)

The synthesis of b4CzBP was based on a method previously reported in literature.³⁶ In a two-neck round bottom flask, carbazole (2 eq, 18.6 mmol, 3.1078 g) and potassium *tert*-butoxide (3 eq, 27.9 mmol, 3.1248g) were dissolved in 50 mL of anhydrous DMF under an argon atmosphere. An 25 mL solution of bis(4-fluorophenyl)methanone (1 eq, 9.3 mmol, 2.0274 g) in DMF was prepared separately and added dropwise to the two-neck round bottom flask under an argon atmosphere. The reaction mixture was refluxed for 10 hours, brought down to room temperature, and slowly poured into 100 mL of ice water. The resulting yellow precipitate was filtered off, rinsed with ethanol, and dried under vacuum. The solid was then dissolved in DCM, and extracted with an aqueous solution of LiCl (5%) three times to remove residual DMF. The DCM layer was dried over MgSO₄ and filtered through a cotton plug. The DCM was removed by rotary evaporation, which yielded 3.5623 g (74% yield) of a light yellow solid.

(4-Methoxyphenyl)[4-(trifluoromethyl)phenyl]methanone (4-MeO-4'-CF₃ BP)

The synthesis of 4-MeO-4'-CF₃ BP was based on a method previously reported in literature.³⁴ A two-neck, 50 mL round bottom flask was charged with a stir-bar and Mg turnings (16.1 mmol, 0.3907 g) was oven dried for 30 minutes. The flask was evacuated

and back-filled with argon three times. Then, under flow of argon, 4-bromobenzotrifluoride (1 eq, 10.7 mmol, 1.5 mL) was added dropwise to the flask, followed by 25 mL of freshly distilled THF. The flask was sonicated for 10 minutes to help initiate the reaction. Bubbles were seen forming at the surface of the Mg turnings. This solution was stirred at room temperature for 4 hours under argon flow, and was subsequently added dropwise to a solution of 4-methoxybenzaldehyde (1.4 eq, 15.1 mmol, 1.3 mL) in THF (10 mL) that was chilled to -78°C in a dry-ice/acetone bath. The reaction was stirred for 8 hours, during which it was allowed to warm up to room temperature. The reaction was subsequently quenched with aqueous HCl (2 M) and extracted three times with ethyl acetate. The ethyl acetate layer was washed with brine, dried over MgSO_4 , and the solvent removed by rotary evaporation. The resulting residue was diluted with DCM (10 mL) and added to a mixture of pyridinium chlorochromate (2 eq, 13 mmol, 2.808 g) and silica gel (3.745 g) in DCM (10 mL). The reaction was stirred and monitored by TLC until completion. The reaction mixture was filtered through a silica plug, resulting in a light-yellow solution. The solvent was removed by rotary evaporation, and the resulting off-white solid was recrystallized from a 1:1 mixture of DCM and hexanes, which yielded 2.1 g (70 % yield) of a crystalline, off-white solid.

2.3.3 Synthesis of $\text{Ni}(\text{NO}_3)_2\text{dtbby}$

$\text{Ni}(\text{NO}_3)_2 \cdot 6\text{H}_2\text{O}$ (1.5 eq, 500.1 mg, 2.7 mmol) was added to a two-necked round bottom flask with a stir bar. The flask was evacuated and backfilled with argon three times and left under argon flow. Freshly distilled THF (50 mL) was added to the flask and the temperature was increased to 50°C . Then, 4,4'-Di-tert-butyl-2,2'-dipyridyl (1 eq,

488.9 mg, 1.8 mmol) was added to a separate round bottom flask, which was subsequently evacuated and backfilled with argon three times. Under argon flow, THF (100 mL) was added to the flask containing 4,4'-Di-tert-butyl-2,2'-dipyridyl and the solution was drawn up in a syringe and added dropwise to the flask containing $\text{Ni}(\text{NO}_3)_2 \cdot 6\text{H}_2\text{O}$ and the mixture was left to stir at 50 °C for 30 minutes. The solvent was then removed by rotary evaporation, leaving behind a blue residue that was recrystallized via slow mixing of THF and hexanes. To the residue was added diethyl ether (50 mL) and the solution was heated to reflux until the residue dissolved, after which the solution was left to cool to room temperature to induce the formation of a light-blue, crystalline powder. The nickel complex is sufficiently pure to be used in catalytic reactions at this point.

For single crystal x-ray diffraction analysis, 30 mg of the complex was redissolved in a minimal amount of THF (~0.5 mL) and placed in a screw top vial. Hexane (1.5 mL) was slowly layered on top of the THF layer and the vial was left undisturbed for about three days and translucent-blue plate crystals were harvested from the bottom and walls of the vial.

2.4 Conclusions and Future Direction

A photochemical methodology for the coupling of aryl halides (bromides, chlorides, and iodides) and THF using a class of benzophenone-derived organic molecules as photocatalysts has been elucidated. These ketones are either commercially available or easily prepared from widely available starting materials. The reaction pathway is different than what has been previously reported using iridium-centered

photocatalysts^{2 1}, and appears to proceed through a HAT/SET photocatalytic cycle which is coupled to the catalytic nickel redox cycle that mediates C-C bond formation. The method produces the desired cross-coupled product in yields up to 97% for aryl bromides, and features an option for yield improvement of up to 94% for aryl chlorides using 0.5 eq TBA-Br as an additive. The strong utility of our methodology is further highlighted by reaction times ranging from 36-72 hours and conditions that allow the reaction to be run at room temperature without the use of expensive heavy metals or strong oxidants or reductants.

However, there are still some limitations that can be expanded upon. Aryl iodides perform poorly as substrates in this reaction. The performance of aryl chlorides was drastically improved in the presence of TBA-Br. While the yields from aryl iodides did not seem to respond to TBA-Br, perhaps a more in-depth screening of halide additives could improve upon their performance. The substrate scope could also be expanded to further assess the viability of this method in natural product synthesis.

Appendix A

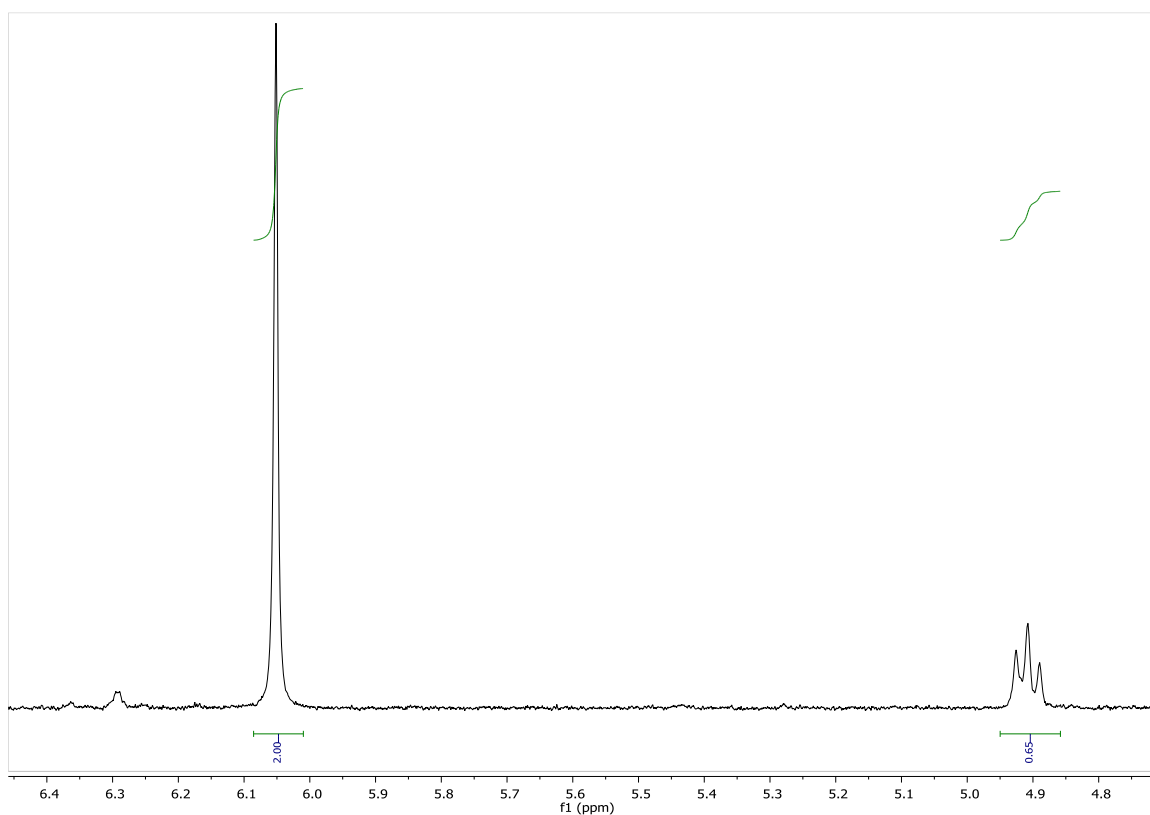


Figure 8. ^1H NMR spectrum of crude reaction mixture using b4CzBP showing integration ratios between product proton and internal standard protons. Internal standard=2,4,6-trimethoxybenzonitrile.

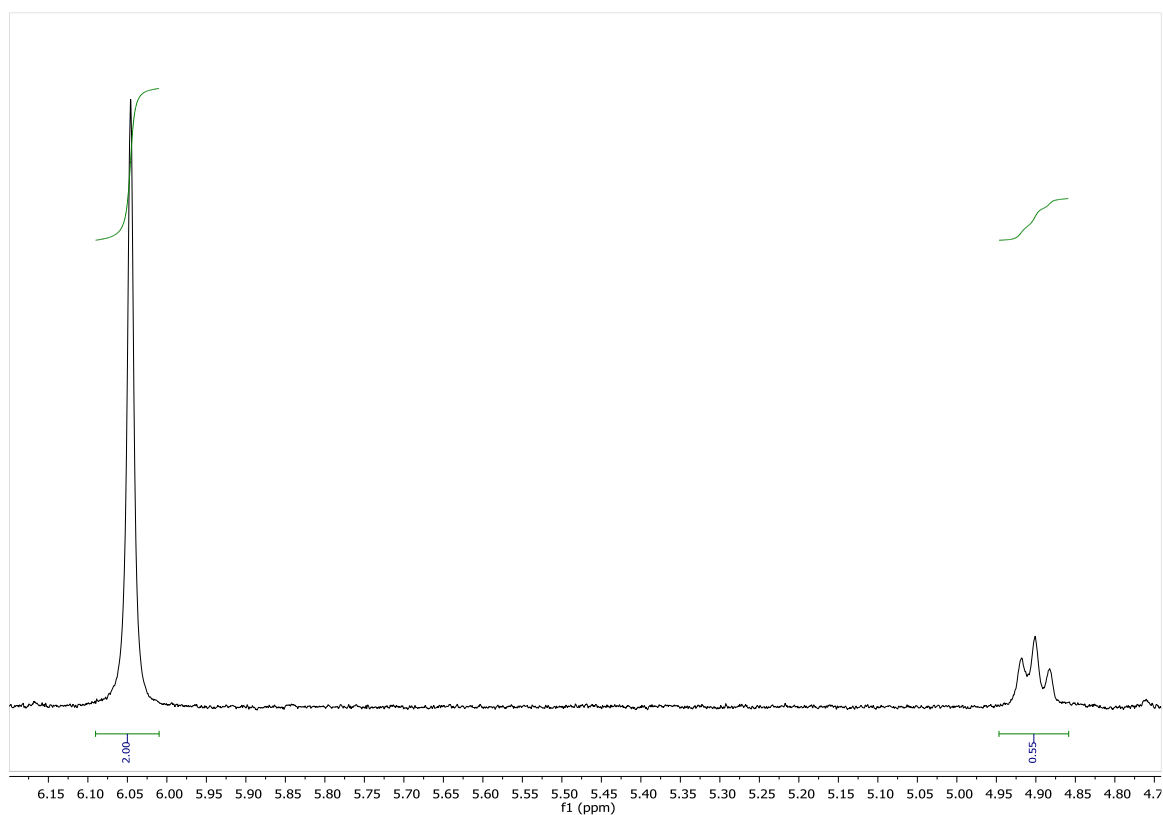


Figure 9. ^1H NMR spectrum of crude reaction mixture using $\text{Ir}[\text{dF}(\text{CF}_3)\text{ppy}]_2\text{dtbbpy}]\text{PF}_6$ showing integration ratios between product proton and internal standard protons.

Figure 10. ^1H NMR spectrum of product isolated from reaction using b4CzBP as the photocatalyst.

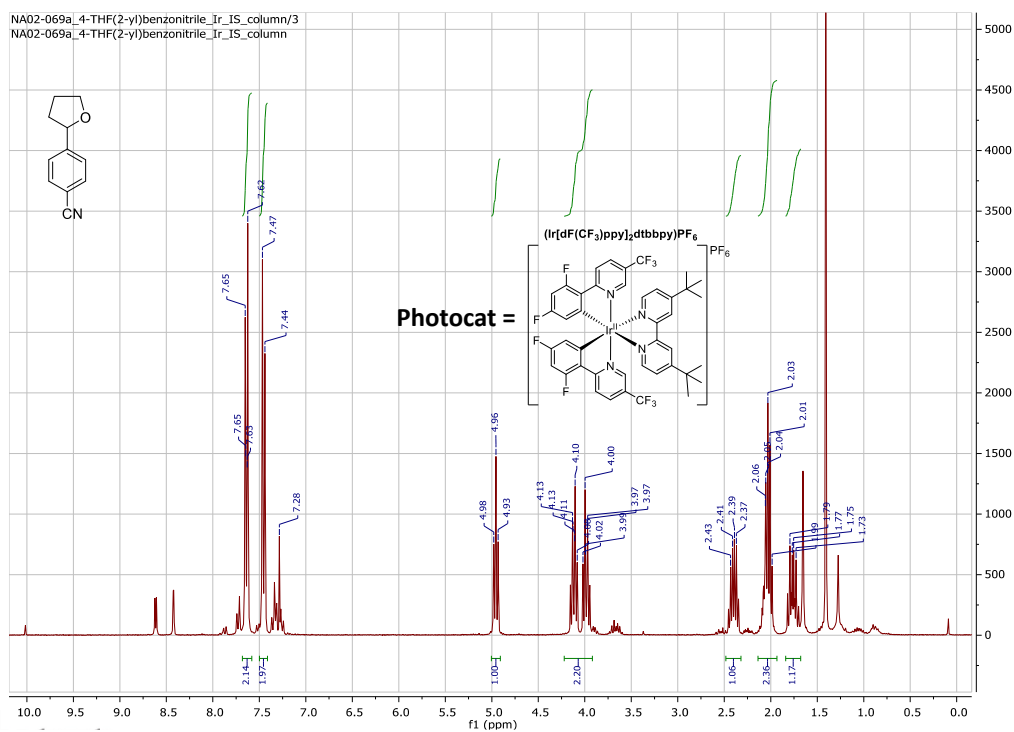


Figure 11. ^1H NMR spectrum of product isolated from reaction using $\text{Ir}[\text{dF}(\text{CF}_3)\text{ppy}]_2\text{dtbbpy}]\text{PF}_6$ as the photocatalyst.

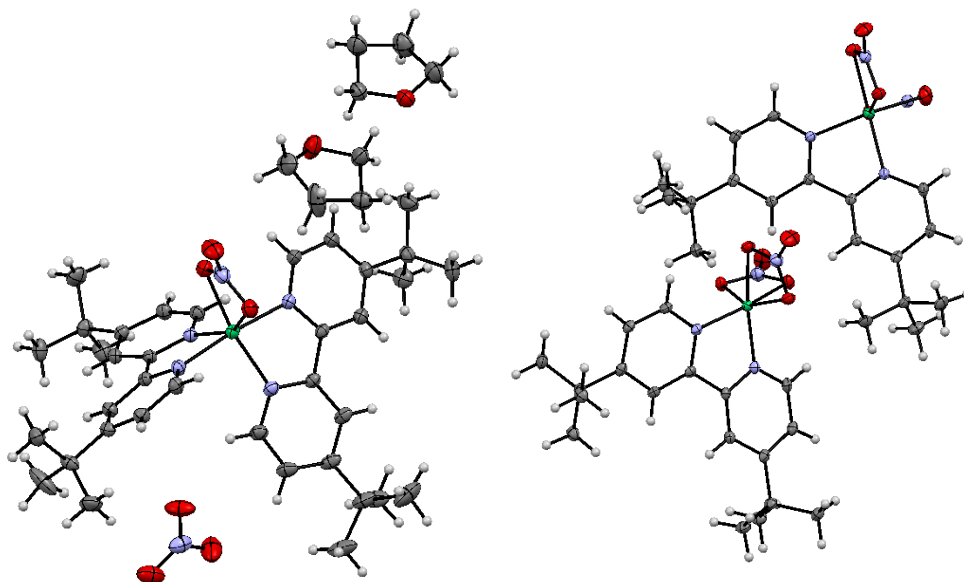


Figure 12. Single-crystal XRD characterization of $\text{Ni}(\text{NO}_3)(\text{dtbbpy})_2$ [left] and $\text{Ni}(\text{NO}_3)_2(\text{dtbbpy})$ [right].

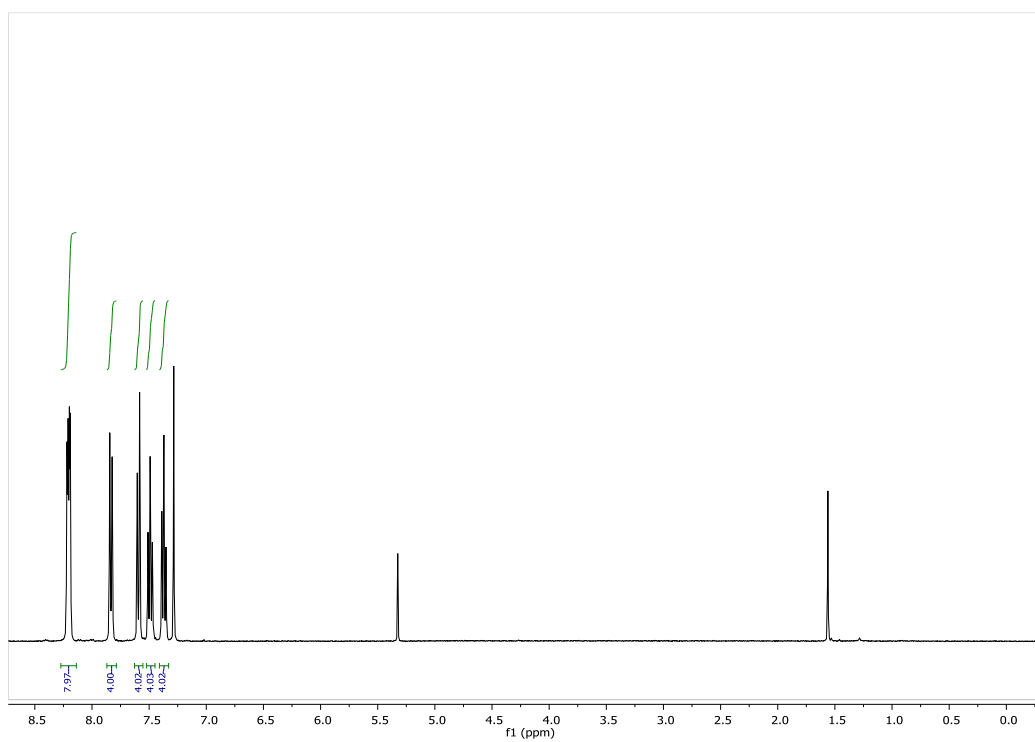


Figure 13. ^1H NMR of b4CzBP.

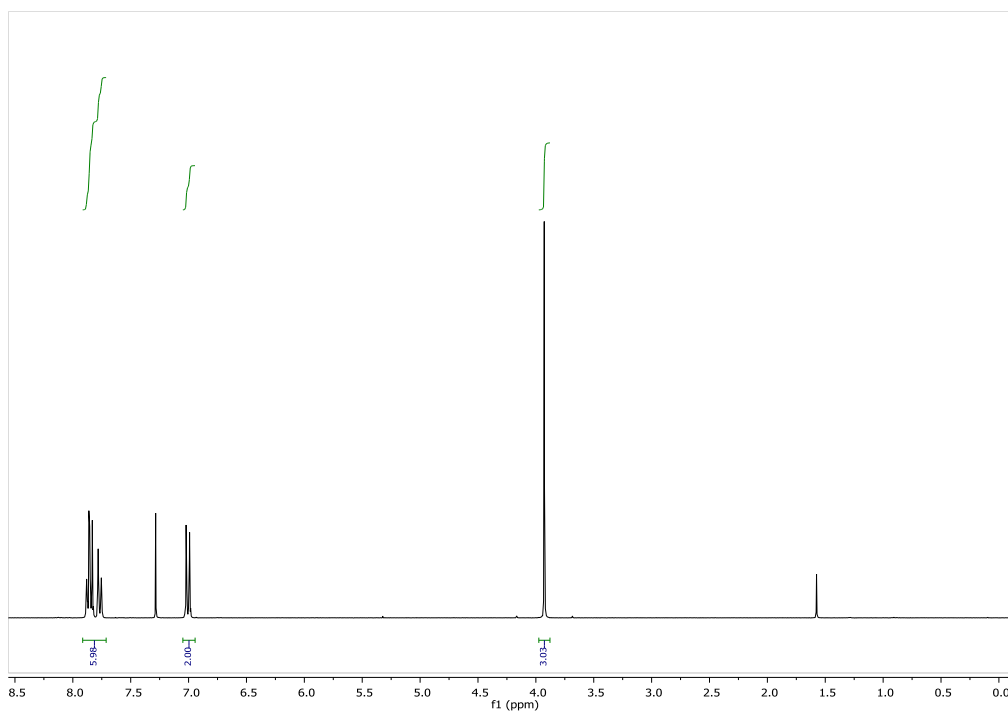


Figure 14. ^1H NMR of 4-MeO-4'-CF₃ BP

References

1. Heitz, D. R.; Tellis, J. C.; Molander, G. A., Photochemical Nickel-Catalyzed C-H Arylation: Synthetic Scope and Mechanistic Investigations. *J Am Chem Soc* **2016**, *138* (39), 12715-12718.
2. Shields, B. J.; Doyle, A. G., Direct C(sp³)-H Cross Coupling Enabled by Catalytic Generation of Chlorine Radicals. *J Am Chem Soc* **2016**, *138* (39), 12719-12722.
3. Hasegawa, N.; Charra, V.; Inoue, S.; Fukumoto, Y.; Chatani, N., Highly Regioselective Carbonylation of Unactivated C(sp³)-H Bonds by Ruthenium Carbonyl. *Journal of the American Chemical Society* **2011**, *133* (21), 8070-8073.
4. Sundararaju, B.; Achard, M.; Sharma, G. V. M.; Bruneau, C., sp³ C-H Bond Activation with Ruthenium(II) Catalysts and C(3)-Alkylation of Cyclic Amines. *Journal of the American Chemical Society* **2011**, *133* (27), 10340-10343.
5. Huang, X.; Wang, Y.; Lan, J.; You, J., Rhodium(III)-Catalyzed Activation of C-H Bonds and Subsequent Intermolecular Amidation at Room Temperature. *Angewandte Chemie International Edition* **2015**, *54* (32), 9404-9408.
6. Wang, X.; Yu, D.-G.; Glorius, F., Cp*Rh(III)-Catalyzed Arylation of C(sp³)-H Bonds. *Angewandte Chemie International Edition* **2015**, *54* (35), 10280-10283.
7. Pan, J.; Su, M.; Buchwald, S. L., Palladium(0)-Catalyzed Intermolecular Amination of Unactivated C-H Bonds. *Angewandte Chemie International Edition* **2011**, *50* (37), 8647-8651.
8. Zaitsev, V. G.; Shabashov, D.; Daugulis, O., Highly Regioselective Arylation of sp³ C-H Bonds Catalyzed by Palladium Acetate. *Journal of the American Chemical Society* **2005**, *127* (38), 13154-13155.
9. Roy, J., Pharmaceutical impurities--a mini-review. *AAPS PharmSciTech* **2002**, *3* (2), E6-E6.
10. Ahuja, S., Assuring quality of drugs by monitoring impurities. *Advanced Drug Delivery Reviews* **2007**, *59* (1), 3-11.
11. Garrett, C. E.; Prasad, K., The Art of Meeting Palladium Specifications in Active Pharmaceutical Ingredients Produced by Pd-Catalyzed Reactions. *Advanced Synthesis & Catalysis* **2004**, *346* (8), 889-900.
12. Welin, E. R.; Warkentin, A. A.; Conrad, J. C.; MacMillan, D. W. C., Enantioselective α -Alkylation of Aldehydes by Photoredox Organocatalysis: Rapid Access to Pharmacophore Fragments from β -Cyanoaldehydes. *Angewandte Chemie International Edition* **2015**, *54* (33), 9668-9672.
13. McNally, A.; Prier, C. K.; MacMillan, D. W. C., Discovery of an α -Amino C-H Arylation Reaction Using the Strategy of Accelerated Serendipity. *Science* **2011**, *334* (6059), 1114-1117.
14. Terrett, J. A.; Cuthbertson, J. D.; Shurtleff, V. W.; MacMillan, D. W. C., Switching on elusive organometallic mechanisms with photoredox catalysis. *Nature* **2015**, *524* (7565), 330-334.
15. Tasker, S. Z.; Jamison, T. F., Highly Regioselective Indoline Synthesis under Nickel/Photoredox Dual Catalysis. *Journal of the American Chemical Society* **2015**, *137* (30), 9531-9534.

16. Shaw, M. H.; Twilton, J.; MacMillan, D. W., Photoredox Catalysis in Organic Chemistry. *J Org Chem* **2016**, *81* (16), 6898-926.
17. Neufeldt, S. R.; Sanford, M. S., Combining Transition Metal Catalysis with Radical Chemistry: Dramatic Acceleration of Palladium-Catalyzed C–H Arylation with Diaryliodonium Salts. *Advanced Synthesis & Catalysis* **2012**, *354* (18), 3517-3522.
18. Lang, S. B.; O’Nele, K. M.; Tunge, J. A., Decarboxylative Allylation of Amino Alkanoic Acids and Esters via Dual Catalysis. *Journal of the American Chemical Society* **2014**, *136* (39), 13606-13609.
19. Kalyani, D.; McMurtrey, K. B.; Neufeldt, S. R.; Sanford, M. S., Room-Temperature C–H Arylation: Merger of Pd-Catalyzed C–H Functionalization and Visible-Light Photocatalysis. *Journal of the American Chemical Society* **2011**, *133* (46), 18566-18569.
20. Zuo, Z.; Ahneman, D. T.; Chu, L.; Terrett, J. A.; Doyle, A. G.; MacMillan, D. W. C., Merging photoredox with nickel catalysis: Coupling of α -carboxyl sp³-carbons with aryl halides. *Science* **2014**, *345* (6195), 437-440.
21. Tellis, J. C.; Primer, D. N.; Molander, G. A., Single-electron transmetalation in organoboron cross-coupling by photoredox/nickel dual catalysis. *Science* **2014**, *345* (6195), 433-436.
22. Ye, Y.; Sanford, M. S., Merging Visible-Light Photocatalysis and Transition-Metal Catalysis in the Copper-Catalyzed Trifluoromethylation of Boronic Acids with CF₃I. *Journal of the American Chemical Society* **2012**, *134* (22), 9034-9037.
23. Ratani, T. S.; Bachman, S.; Fu, G. C.; Peters, J. C., Photoinduced, Copper-Catalyzed Carbon–Carbon Bond Formation with Alkyl Electrophiles: Cyanation of Unactivated Secondary Alkyl Chlorides at Room Temperature. *Journal of the American Chemical Society* **2015**, *137* (43), 13902-13907.
24. Creutz, S. E.; Lotito, K. J.; Fu, G. C.; Peters, J. C., Photoinduced Ullmann C–N Coupling: Demonstrating the Viability of a Radical Pathway. *Science* **2012**, *338* (6107), 647-651.
25. Bissember, A. C.; Lundgren, R. J.; Creutz, S. E.; Peters, J. C.; Fu, G. C., Transition-Metal-Catalyzed Alkylations of Amines with Alkyl Halides: Photoinduced, Copper-Catalyzed Couplings of Carbazoles. *Angewandte Chemie International Edition* **2013**, *52* (19), 5129-5133.
26. Sahoo, B.; Hopkinson, M. N.; Glorius, F., Combining Gold and Photoredox Catalysis: Visible Light-Mediated Oxy- and Aminoarylation of Alkenes. *Journal of the American Chemical Society* **2013**, *135* (15), 5505-5508.
27. Hopkinson, M. N.; Sahoo, B.; Glorius, F., Dual Photoredox and Gold Catalysis: Intermolecular Multicomponent Oxyarylation of Alkenes. *Advanced Synthesis & Catalysis* **2014**, *356* (13), 2794-2800.
28. Cheng, Y.; Yang, J.; Qu, Y.; Li, P., Aerobic Visible-Light Photoredox Radical C–H Functionalization: Catalytic Synthesis of 2-Substituted Benzothiazoles. *Organic Letters* **2012**, *14* (1), 98-101.
29. Fukuzumi, S.; Kotani, H.; Ohkubo, K.; Ogo, S.; Tkachenko, N. V.; Lemmetyinen, H., Electron-Transfer State of 9-Mesityl-10-methylacridinium Ion with a Much Longer Lifetime and Higher Energy Than That of the Natural Photosynthetic Reaction Center. *Journal of the American Chemical Society* **2004**, *126* (6), 1600-1601.

30. Luo, J.; Zhang, J., Donor–Acceptor Fluorophores for Visible-Light-Promoted Organic Synthesis: Photoredox/Ni Dual Catalytic C(sp³)–C(sp²) Cross-Coupling. *ACS Catalysis* **2016**, *6* (2), 873-877.
31. Murai, H.; Jinguji, M.; Obi, K., Activation energy of hydrogen atom abstraction by triplet benzophenone at low temperature. *The Journal of Physical Chemistry* **1978**, *82* (1), 38-40.
32. Luo, J.; Zhang, J., Aerobic Oxidation of Olefins and Lignin Model Compounds Using Photogenerated Phthalimide-N-oxyl Radical. *The Journal of organic chemistry* **2016**, *81* (19), 9131-9137.
33. Hoffmann, N., Photochemical Electron and Hydrogen Transfer in Organic Synthesis: The Control of Selectivity. *Synthesis* **2016**, *48* (12), 1782-1802.
34. Shen, Y.; Gu, Y.; Martin, R., sp³ C–H Arylation and Alkylation Enabled by the Synergy of Triplet Excited Ketones and Nickel Catalysts. *Journal of the American Chemical Society* **2018**, *140* (38), 12200-12209.
35. Dewanji, A.; Krach, P. E.; Rueping, M., The Dual Role of Benzophenone in Visible-Light/Nickel Photoredox-Catalyzed C–H Arylations: Hydrogen-Atom Transfer and Energy Transfer. *Angewandte Chemie International Edition* **2019**, *58* (11), 3566-3570.
36. Huang, W.; Zhou, H.; Li, B.; Su, J., New thermally stable cyano-substituted D–A– π –A–D molecules with aggregation-induced emission and large two-photo absorption cross-sections. *RSC Advances* **2013**, *3* (9), 3038-3045.